DOI: 10.1002/chem.201604007



■ Magnetochemistry

Metal-Metal Single Bonds with the Magnetic Anisotropy of Quadruple Bonds: A Systematic Series of Heterobimetallic Bismuth(II)-Rhodium(II) Formamidinate Complexes

Travis L. Sunderland and John F. Berry*[a]

Abstract: The first set of five heterobimetallic MM′(form)₄ (form = formamidinate) complexes containing a BiRh core has been successfully synthesized. The Bi–Rh bond lengths lie between 2.5196(6) and 2.572(2) Å, consistent with Bi–Rh single bonds. All complexes have rich electrochemistry, with the [BiRh]^{4+/5+} redox couples spanning approximately 700 mV and showing a strong correlation to remote ligand

substitution. Visible spectroscopy showed two features for complexes 1–5 at approximately 459 and 551 nm, unique to BiRh paddlewheel complexes that are attributed to LMCT bands into the Bi–Rh σ^* orbital. The large spin–orbit coupling (SOC) of Bi creates a massive Bi–Rh magnetic anisotropy, $\Delta\chi$, approximately -4800×10^{-36} m³molecule $^{-1}$, which is the largest value reported for any single bond to date.

Introduction

The diamagnetism of bismuth is unmatched among the stable elements. When combined with magnetic elements, the large diamagnetism and spin-orbit coupling of Bi have recently been shown to engender materials with ferromagnetism and large magnetic anisotropies.^[1] However, discrete coordination complexes, in which heterometallic Bi--M interactions can be directly probed, remain uncommon.^[2] In 2005, Dikarev et al. reported a synthetic breakthrough allowing access to carboxylate complexes with Bi-Rh single bonds. [3] Further development of solution routes to these complexes has opened up access to a wide variety of BiRh carboxylate and oxypyridinate compounds.^[4] We now report a systematic series of new BiRh compounds, the first to be supported by (N,N) donor formamidinate ligands, which allows us to contrast two important properties of Rh-Rh and Bi-Rh single bonds, namely, their redox chemistry and their magnetic anisotropy ($\Delta\chi$ (measured in units of 10^{-36} m³molecule⁻¹), in which χ is magnetic susceptibility). Typically, large values of $\Delta \chi$ are expected for molecules with an element-element multiple bond. Recent work^[5] on the impact of bond polarity on $\Delta \chi$ has prompted us to measure $\Delta \chi$ for the Bi–Rh single bond, and we report herein that $\Delta \chi$ is exceptionally large in this case.

Results and Discussion

Synthesis and characterization

Complexes 1–5 were synthesized by combining BiRh(TFA)₄^[4a] (TFA = trifluoroacetate) with an excess of H(form) (form = formamidinate) and heating the mixture above the melting point of the ligand under a static vacuum, which caused a color change from yellow to red brown upon equatorial ligand exchange (Scheme 1). The ¹H NMR spectra of 1–5 in CDCl₃ are all

$$\begin{pmatrix} CF_3 \\ O O O \\ Bi - Rh \end{pmatrix} \xrightarrow[H]{} R = OMe (1), Me (2), H (3), CI (4), CF_3 (5)$$

Scheme 1. General reaction conditions to synthesize 1-5.

consistent with C_{4v} symmetry on the NMR time scale, in which the four equatorial ligands are symmetry equivalent, but the phenyl rings and associated *para* substituents from an individual formamidinate ligand are inequivalent due to the heterobimetallic BiRh core. The methine H atoms appear as doublets due to coupling to the ¹⁰³Rh nucleus (100% abundance, $I=^1/_2$, $^3J_{\rm H-Rh}\approx 1.7$ Hz) and are significantly deshielded due to the magnetic anisotropy of the Bi–Rh single bond, appearing near $\delta=8.5$ ppm in CDCl₃ (see below).

Crystallography

Complexes 1–5 have been crystallographically characterized and are all isostructural with the Rh atom in a square pyramidal geometry with four N atoms bound equatorially and capped by the Bi atom. Likewise, the Bi atom is in a distorted

[[]a] Dr. T. L. Sunderland, Dr. J. F. Berry
Department of Chemistry, University of Wisconsin-Madison
1101 University Ave. Madison, WI 53706 (USA)
E-mail: berry@chem.wisc.edu

Supporting information for this article can be found under http:// dx.doi.org/10.1002/chem.201604007.



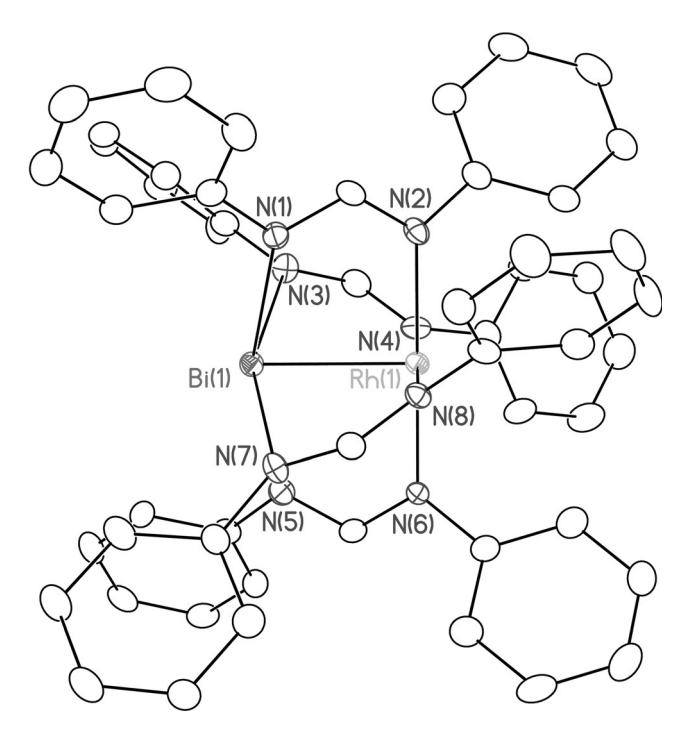


Figure 1. X-ray crystal structure of **3** with thermal ellipsoids drawn at the 50% probability level. Hydrogen atoms have been removed for clarity.

square pyramidal geometry, puckered out of the plane of four N atoms away from the apical Rh atom (see Figure 1, Table 1, and Figures S1–S4 and Tables S1–S6 in the Supporting Information). The Bi–N bonds are all uniformly longer than the Rh–N bonds by 0.4 Å. All complexes have short Bi–Rh bond lengths between 2.5196(6) and 2.572(2) Å, consistent with a Bi–Rh single σ bond (Figure S5 in the Supporting Information). As is observed for other $M_2(form)_4$ compounds, $^{[6]}$ more electron-rich ligands lead to slightly shorter M–M bond lengths. The equatorial ligands also display a significant twisting with N-Bi-Rh-N torsion angles between 18.0[5] and 25.9(5)°.

Table 1. Experimental bond lengths [Å] and angles [°] for 1–5.							
Compd	1 ^[a]	2	3	4	5		
Bi-Rh	2.527(1)	2.5196(6)	2.5279(3)	2.5420(3)	2.5407(2)		
Bi-N _{av}	2.436(7)	2.457(3)	2.451[3]	2.438[2]	2.451[2]		
Rh–N _{av} torsion	2.040(7) 23.7(1)	2.052(3) 25.9(5)	2.051[2] 23.2[5]	2.056[2] 18.0[5]	2.053[2] 18.6[5]		

[a] Presented data are from the non-disordered molecule in the asymmetric unit

Electrochemistry

Metal–metal-bonded complexes often show interesting redox features. Specifically, singly bonded Rh_2 paddlewheel complexes supported by either (O,O), (O,N), or (N,N) donor ligands often display reversible $[Rh_2]^{4+/5+}$ redox couples with the tetracarboxylate complexes spanning a wide range of potentials from 1.06 to -0.345 V versus $Fc/Fc^{+}.^{[7]}$ Heterobimetallic BiRh

www.chemeurj.org

complexes supported by either carboxylate or oxypyridinate ligands both have irreversible [BiRh]^{4+/5+} redox couples at higher potentials than their corresponding Rh₂ complexes.^[4b] In contrast, **1–5**, supported by more basic amidinate ligands, displayed reversible [BiRh]^{4+/5+} redox couples at lower potentials than the corresponding Rh₂ complexes, as shown in Figure 2 and Table 2 (see also Figures S6, S7, and Table S7 in the Supporting Information).

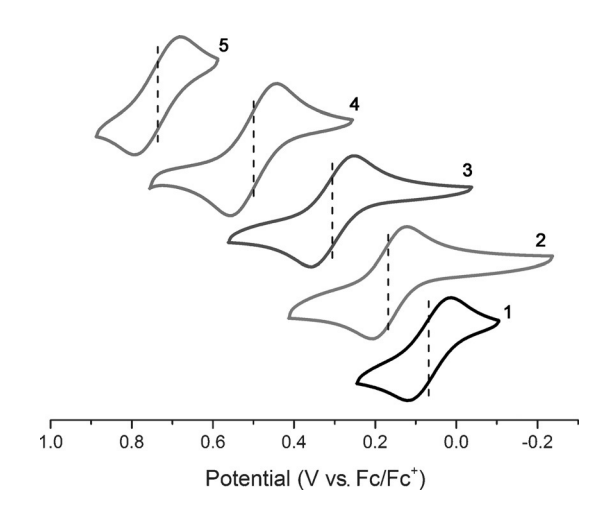


Figure 2. Cyclic voltammograms of **1–5** in CH₂Cl₂ with scan rate 100 mV s⁻¹ (0.1 M tetrabutylammonium hexafluorophosphate (TBAH)).

Table 2. Comparison of electrochemical data ^[a] for compounds 1–5 and Rh ₂ (form) ₄ . ^[b]							
Compd	$[MRh]^{4+/5+} E_{1/2} [mV]$	Ref.					
1	70.6	this work					
2	168	this work					
3	307	this work					
4	502	this work					
5	736	this work					
Rh₂(p-OMe-form)₄	274	8 b					
$Rh_2(p-CH_3-form)_4$	341	8 b					
Rh ₂ (form) ₄	471	8 b					
$Rh_2(p-Cl-form)_4$	667	8 b					
Rh ₂ (p-CF ₃ -form) ₄	891	8 b					

[a] All potentials are versus Fc/Fc^+ in CH_2Cl_2 . [b] form = N, N-diphenylformamidinate; aryl-substituted formamidinate ligands are abbreviated with their corresponding substituents denoted.

Linear free-energy relationships between redox potential and the Hammett parameter (σ) have been established for several homobimetallic formamidinate complexes; however, no such analysis has been made on heterobimetallic formamidinate complexes. Using Equation (1), a reactivity constant (ρ) can be extracted from the electrochemical data, which quantifies the sensitivity the corresponding redox couple experiences from remote substitution on the equatorial ligand. [8f]

$$\Delta E_{(1/2)} = \rho(8\sigma) \,\mathrm{mV} \tag{1}$$





Values of ρ for the $[M_2(form)_4]^{4+/5+}$ couple range from 87–114 mV and are listed above in Table 3. Based on the electronic structure of 1–5, we expect oxidation from $[BiRh]^{4+}$ to $[BiRh]^{5+}$ to be localized on the Rh atom (Figure S5 in the Supporting Information). This localized analysis suggests that all eight aryl substituents may not contribute equally to ρ , and that ρ for BiRh complexes should be smaller than for homobimetallic compounds. Surprisingly, this is not the case: analysis of the electrochemical data for the $[BiRh(form)_4]^{4+/5+}$ couple revealed a ρ value of 102 mV, slightly higher than that for $[Rh_2(form)_4]^{4+/5+}$ (98 mV), $[Rh_2(form)_4]^{4+/5+}$ as shown in Figure 3 and Table 3.

Table 3. Comparison of electrochemical data ^[a] for compounds 1–5 and Rh ₂ (form) ₄ compounds.					
MM(form) ₄	ho [mV]	Ref.			
BiRh	102	this work			
Mo ₂	87	8 c, d			
Rh ₂	98	8 b			
Ni ₂	114	8 a			

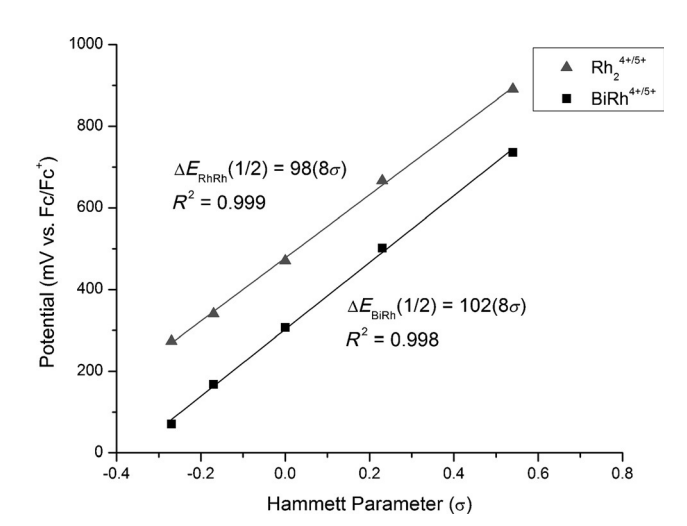


Figure 3. Hammett plots of potential versus σ for [BiRh(form)₄]^{4+/5+} (black squares) and [Rh₂(form)₄]^{4+/5+} (blue triangles) redox couples^(8b) with lines of best fit for each.

UV/Vis spectroscopy

Heterobimetallic BiRh carboxylates and oxypyridinates are featureless in the visible spectrum. Consistent with their more accessible redox couples, 1–5 also have more accessible electronic transitions and are red brown. The UV/Vis spectra for 1–5 are shown in Figure 4. All complexes have a strong absorption feature at approximately 459 nm. A second, weaker, feature at approximately 551 nm is also present for all complexes.

To gain more insight into the electronic structure of BiRh(-form)₄ complexes, spectroelectrochemical measurements were performed on the [BiRh]^{4+/5+} redox couple of 1, which has the most accessible one-electron oxidation from complexes 1–5. The oxidation process was monitored by UV/Vis spectroscopy,

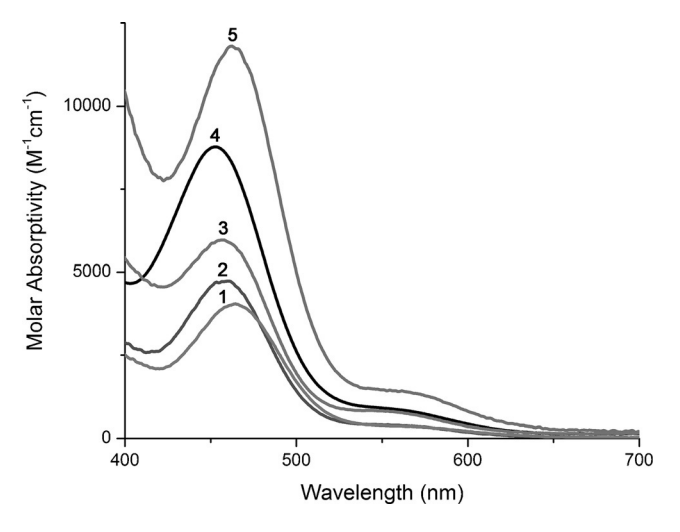


Figure 4. Overlay of UV/Vis spectra for 1-5 in CH₂Cl₂.

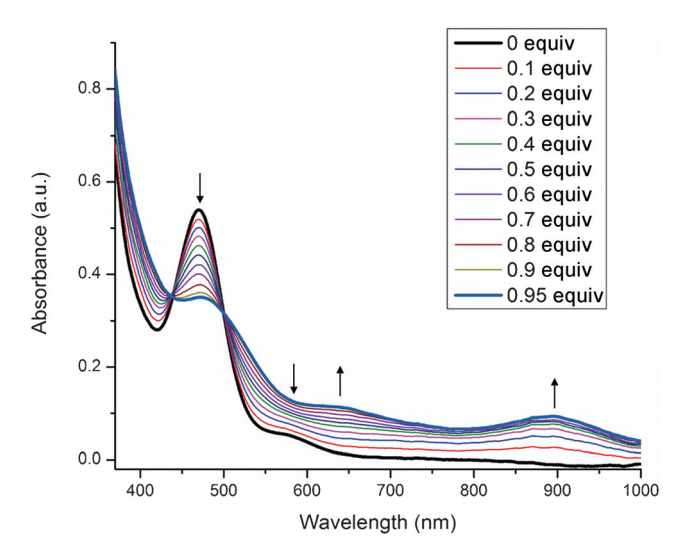


Figure 5. UV/Vis spectra from electrochemical oxidation of 1 in CH₂Cl₂.

as shown in Figure 5. During the oxidation, the red brown solution became darker. The peak of 1 at $\lambda=453$ nm loses intensity and shifts to lower energy. The feature at 544 nm loses intensity followed by the growth of a new feature at slightly lower energy at approximately 645 nm and an additional broad feature at $\lambda\approx900$ nm. The presence of two isosbestic points at 440 and 505 nm indicated a direct conversion of 1 to an isostructural [1]⁺.

DFT calculations

The nature of the transitions of both 1 and [1] $^+$ were investigated with time-dependent (TD) DFT. An overlay of the predicted absorption spectra for both complexes, with remarkable agreement to the experimental spectra, is shown in Figure 6. For complex 1, the band at 575 nm can be assigned as a LMCT band with excitations into the Bi–Rh σ^* orbital (the Bi–Rh σ^* orbital is shown in Figure S8 in the Supporting Information). The higher energy band at 453 nm is a combination of LMCT



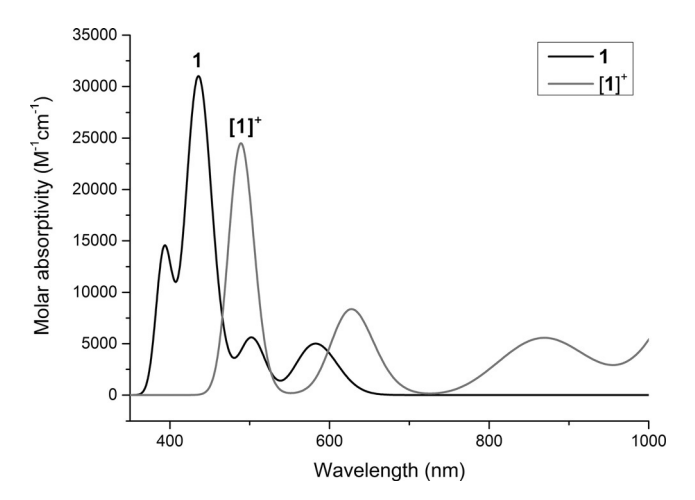


Figure 6. TD-DFT predicted absorption spectra for 1 and [1]⁺.

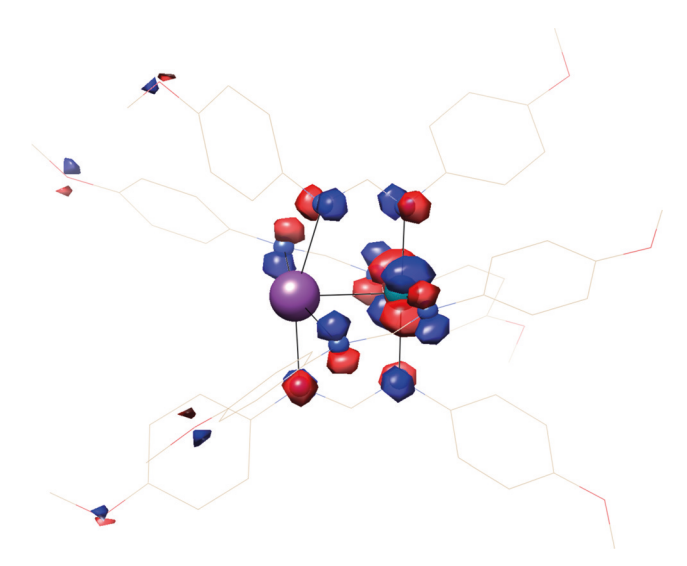


Figure 7. DFT-calculated singly occupied molecular orbital (SOMO) for $[1]^+$, with an approximately 0.05 isodensity cutoff. The sea-green ball is the Rh atom, and the purple ball is the Bi atom. The red/blue colors show the phases of the orbital. The SOMO consists of a 23% contribution from the Rh $4d_{xy}$ orbital, with zero% Bi character.

bands and $d \rightarrow d$ transitions from orbitals localized on the Rh atom. The one-electron oxidation of 1 removed one electron from the HOMO, the resulting singly occupied molecular orbital (SOMO) is shown in Figure 7.

Removal of one electron from the non-bonding δ -type orbital on the Rh atom allowed new lower-energy electronic absorption features to arise, Figure 6, namely, excitations into the singly occupied molecular orbital (SOMO) from orbitals of π symmetry localized on the Rh atom around 875 nm. The features predicted at approximately 620 and 490 nm are assigned as mainly LMCT bands into the Bi–Rh σ^* orbital. The DFT-calculated structures of both 1 and [1] $^+$ showed little structural changes upon oxidation. The Bi–Rh bond elongates slightly from 2.609 to 2.625 Å. The Bi–N equatorial bonds remain essentially unchanged at 2.463 and 2.466 Å, and the Rh–N bonds contract slightly from 2.095 to 2.073 Å. All of these structural

changes are consistent with removal of one electron from the nonbonding σ -type orbital localized on the Rh atom, resulting in a stronger coulombic repulsion between the metal atoms and a slight contraction of the Rh–N bonds to stabilize a higher oxidation state on the Rh atom.

EPR spectroscopy

To confirm the assignment of Rh centered oxidation, an aliquot of [1]⁺ following electrochemical oxidation was collected and frozen in liquid nitrogen. An EPR spectrum of [1]⁺ was obtained at 10 K, shown in Figures 8 and S9 in the Supporting Information. The spectrum displays a rhombic $S=^1/_2$ signal best modeled with g values of g_x =2.105, g_y =2.000, g_z =1.960, and 103 Rh hyperfine coupling constants of $A_{x,Rh}$ =200, $A_{y,Rh}$ =100, and $A_{z,Rh}$ =150 MHz. In comparison to the 103 Rh, $A_{||}$ values for the [Rh₂(p-CH₃-form)₄]⁺ cation of 44–50 MHz, $^{[10]}$ the data for [1]⁺ are in agreement with a one-electron-oxidized species, in which the single unpaired electron is clearly localized on the Rh atom.

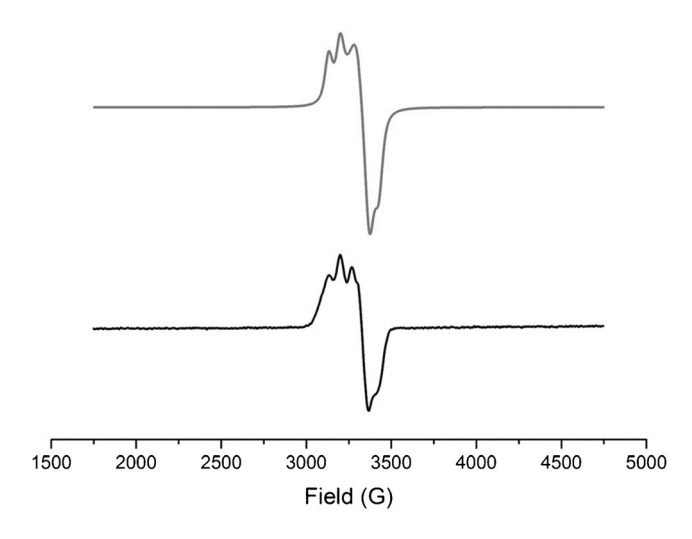


Figure 8. EPR experimental (bottom) and simulated (top) spectra for [1] $^+$ in CH $_2$ Cl $_2$ at 10 K.

Magnetic anisotropy

The ^1H NMR spectroscopy data for **1–5** can be analyzed to determine the magnetic anisotropy of the compounds, $\Delta\chi$, using the model first introduced by McGlinchey. $^{[11]}$ In this model, the NMR chemical shifts are affected by $\Delta\chi$, $^{[12]}$ resulting in two spatial zones, shielding $(-\delta)$ and deshielding $(+\delta)$, signified by the double cone shown in Figure 9 for MM(form)_4 complexes. Notably, the methine H atom of the form ligand resides in the $-\delta$ zone fairly close to the M_2 centroid, and has therefore been used as a sensitive probe for $\Delta\chi$ in a broad range of $M_2(\text{form})_4$ compounds. $^{[6,8b,c,13]}$ The known examples of these are given in Table 4.

The $\Delta\chi$ of the complexes in Table 4 is calculated according to Equation (2), in which $\Delta\delta$ is the difference in ¹H NMR chemical shift of an H atom on the complex of interest and a reference complex without a M–M bond (traditionally, Ni₂(form)₄



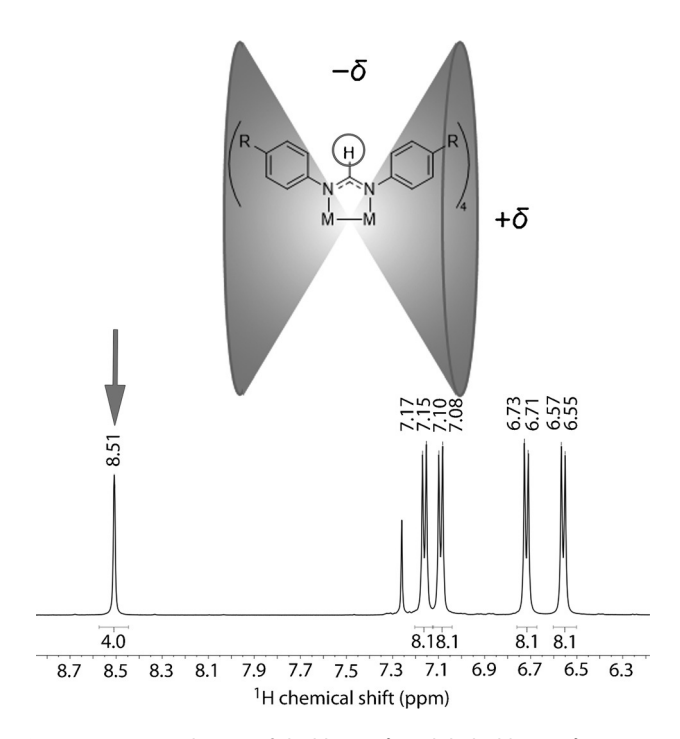


Figure 9. Top: Spatial zones of shielding $(-\delta)$ and deshielding $(+\delta)$ arising from the magnetic anisotropy of the M–M bond. Bottom: Aryl region of the 1 H NMR spectrum of **4**, with the methine proton highlighted.

Table 4. Magnetic anisotropy values derived for **1–5** compared to the other known metal–metal-bonded compounds.

Compd	$\Delta\chi$ [10 ⁻³⁶ m ³ molecule ⁻¹]	Bond order	Ref.
1	-4663	1	this work
2	-4611	1	this work
3	-4729	1	this work
4	-4876	1	this work
5	-4862	1	this work
$Rh_2(p-CH_3-form)_4^{[a]}$	$-2902^{[b]}$	1	8 b, 13 f
Rh ₂ (form) ₄	-2689 ^[b]	1	8b, 13a
Co ₂ (p-OMe-form) ₄	-3877 ^[b]	1	13 b
Pt ₂ (form) ₄ Cl ₂	$-3222^{[b]}$	1	13 c
Cr ₂ (p-CH ₃ -form) ₄	-5230	4	13 d
$Mo_2(p-CH_3-form)_4$	-5060	4	8 c
$W_2(p-CH_3-form)_4$	-5480	4	13 d
$Re_2(p-CH_3-form)_4Cl_2$	-4430	4	13 e
$Ru_2(p-CH_3-form)_4$	-3780	2	13 e
$V_2(p\text{-CH}_3\text{-form})_4$	-7300	3	13 g
Cr ₂ L ^{-[c]}	-3500	5	5 b
MnCrL ^[c]	-3900	5	5 b
FeCrL ^{+[c]}	-5800	3 ^[d]	5 b
C≡C	-340	3	15
C=O	420	2	15
N = O	1300	2	15

[a] form = N,N-diphenylformamidinate; aryl-substituted formamidinate ligands are abbreviated with their corresponding substituents denoted. [b] Calculated from data within the reference. [c] $L = (N(o-(NCH_2PiP_2)C_6H_4)_3)$. [d] Bond order lies between 3–5.

has been used as the reference complex): r (Å) is the distance from the H atom to the centroid of the M—M bond, and θ is the acute angle between the H atom, the centroid of the M—M bond, and the M atom. ^[14]

$$\Delta \delta = \left(\frac{1}{3r^3}\right) \frac{\left(\chi_{\parallel} - \chi_{\perp}\right) [1 - 3\cos^2(\theta)]}{4\pi} \tag{2}$$

The $\Delta\chi$ values of **1–5** are given in Table 4 along with those of reference compounds. It was expected that $\Delta\chi$ should depend on the M–M bond order; additionally, Bill, Gagliardi, Lu and co-workers have suggested that the polarity of M–M bonds in heterobimetallic species can affect $\Delta\chi$. The range of $\Delta\chi$ for homobimetallic M–M singly bonded complexes is -(2700-3900) for Rh₂(form)₄, [8b,13a] Co₂(form)₄, [13b] and Pt₂(form)₄Cl₂. Surprisingly, despite a fairly nonpolar Bi–Rh bond, the heterobimetallic complexes **1–5** display the highest known $\Delta\chi$ values for single bonds (–4800), which places the magnetic anisotropy of these complexes in the range more commonly expected of quadruply bonded complexes. [8c,13d,e]

There are a number of unusual features of the data in Table 4, which become even more apparent when most of the known $\Delta\chi$ values from the literature are plotted as a function of M–M bond order (Figure 10). In organic compounds, $|\Delta\chi|$ increases with bond order (from 140 to 150 to 340 for C–C, C=C, and C=C bonds, respectively, in units of 10^{-36} m³molecule $^{-1}$),^[15] but no such simple relationship exists in M₂ compounds of varying bond orders.

To explain the trend seen in Table 4 and Figure 10, we recall that the magnetic susceptibility, χ , is the sum of diamagnetic (χ_D) and paramagnetic (χ_P) contributions [Eq. (3)]:^[16]

$$\chi = \chi_D + \chi_P \tag{3}$$

Paired electrons contribute to χ_D , with higher bond orders having a larger χ_D due to the ring currents based on the number of electron pairs of the multiple bond. The S=0 ground state of the multiply bonded compounds gives a vanishing first-order Zeeman contribution to χ_P . However, second-

order Zeeman terms of the form $\sum_{n\neq 0} \frac{\langle \psi_o | \hat{\mu}_z | \psi_n \rangle^2}{\mathcal{E}_n - \mathcal{E}_n}$ do not vanish

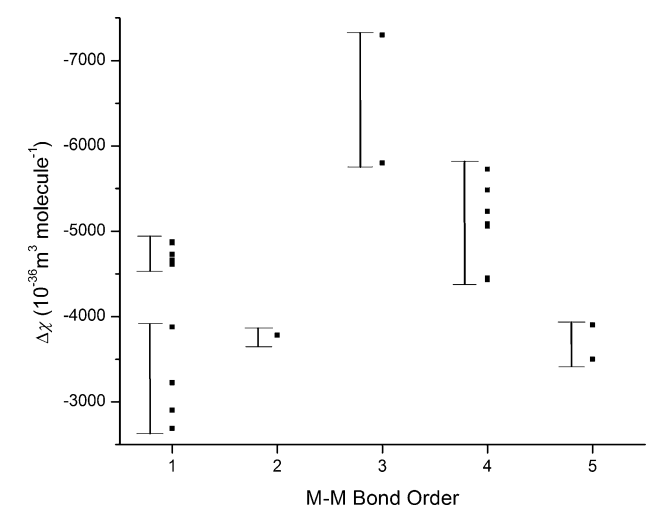


Figure 10. Plot of magnetic anisotropy ($\Delta\chi$ (10^{-36} m³molecule $^{-1}$)) versus M-M bond order for several M-M bonded complexes.



(herein, ψ_o and ψ_n are ground- and excited-state wavefunctions with E_0 and E_n being their energies; \hat{H}_z is the Zeeman Hamiltonian, $\hat{H}_z = \beta(\hat{L} + g\hat{S}) \cdot H$, with $\beta =$ the Bohr magneton, \hat{L} and \hat{S} being orbital and spin angular momentum operators, respectively, q is the Landé factor, and H= applied magnetic field). These second-order Zeeman terms describe field-induced mixing of the ground state with non-thermally populated excited states, resulting in a non-zero temperature-independent contribution to χ_P , called temperature-independent paramagnetism (TIP). Similar to χ_D , χ_P is anisotropic and must be described as a tensor. TIP of diamagnetic compounds should therefore contribute to measured $\Delta \chi$ values, which could either reinforce or counterbalance the diamagnetic anisotropy. Two important properties of molecules can facilitate excited state mixing and therefore increase the contribution of χ_P : relatively small ΔE values, with $\Delta E = E_0 - E_n$, and large spinorbit coupling (SOC). By revisiting the data in Table 4 and Figure 10 with these concepts in mind, for the series of Group 6 $M_2(p\text{-CH}_3\text{-form})_4$ compounds, the trend in $|\Delta\chi|$ of Mo₂ < Cr₂ < W₂ may at first glance appear puzzling. However, it appears that both Cr_2 and W_2 compounds have stronger χ_P contributions to $\Delta \chi$ than does Mo₂(p-CH₃-form)₄, which we attribute to the TIP anisotropy acting to reinforce the diamagnetic anisotropy. If we only consider SOC, we would expect the trend in $|\Delta \chi|$ to be $Cr_2 < Mo_2 < W_2$, which does explain why the W₂ molecule has the largest $|\Delta\chi|$. However, for the Cr₂ molecule, ΔE becomes important, because it is known that Cr_2 quadruple bonds are weak and have several low-lying excited states. [18] This ΔE analysis likely contributes to the large $\Delta \chi$ values of all first-row metal dimers.

In the case of the present BiRh compounds, the apparently large $\Delta \chi$ for these compounds can be attributed to a paramagnetic SOC contribution to the methine chemical shifts. Thus, unlike in organic molecules with large ΔE and small SOC, [19] the data presented in Table 4 and Figure 10 for metal-metalbonded compounds are highly influenced by χ_P contributions to $\Delta \chi$, and no simple trend in bond order exists. However, if we consider only the systematic series of M₂(p-CH₃-form)₄ compounds with second-row metal atoms Mo₂, Ru₂, and Rh₂ for which neither ΔE or SOC contributions are dominant, we do see the expected increase of $|\Delta\chi|$ with bond order from 2902 (Rh₂, single bond) to 3780 (Ru₂, double bond) to 5060 (Mo₂, quadruple bond). At this time, it is unfortunately not possible to disentangle χ_D and χ_P contributions to $\Delta \chi$, although a variable-field NMR spectroscopy study may allow this in future work. To reflect this ambiguity, we suggest that $\Delta \chi$ is best described henceforth as "magnetic anisotropy" rather than the more traditional term "diamagnetic anisotropy".

Conclusion

The inclusion of Bi into BiRh(form)₄ dimers gives strongly colored compounds with unusually accessible redox properties and creates a massive magnetic anisotropy reflected in chemical-shift changes similar to those seen in quadruply bonded metal dimers. The large $\Delta\chi$ values seen for BiRh dimers are attributed to strong paramagnetic second-order Zeeman effects amplified by the large SOC of Bi.

Experimental Section

Materials and methods

All reactions were carried out using oven-dried glassware under a dry N₂ atmosphere by using Schlenk techniques and glovebox methods. BiRh(TFA)₄ (TFA = trifluoroacetate) was prepared according to literature procedures.^[16] The Hform (form = di-aryl-formamidinate) ligands were prepared according to known procedures. [20] The ligand H(p-OMe-form) was purified by sublimation under reduced pressure prior to use. Hexane, ethyl acetate (EtOAc), dichloromethane (DCM), acetonitrile (MeCN), deuterated chloroform (CDCl₃), diethyl ether (Et₂O), and tetrahydrofuran (THF) were purchased from Sigma-Aldrich and used without further purification. ¹H and ¹³C (¹H) NMR spectra were recorded on a Bruker Avance 500 MHz spectrometer at 500 and 125 MHz, respectively. The ¹⁹F{¹H} NMR spectrum was recorded on a Bruker Avance 400 MHz spectrometer at 376 MHz. ¹H and ¹³C{¹H} NMR shifts were referenced to residual proteo solvent, ¹⁹F{¹H} NMR shifts were referenced from the corresponding ¹H NMR frequency. ¹H splitting patterns are designated as doublet (d), multiplet (m), singlet (s), doublet of doublets (dd), triplet (t), and quartet (q). Cyclic voltammetry was performed in 10 mL DCM solutions containing 0.1 м tetrabutylammonium hexafluorophosphate (ТВАН) with 1 mм analyte. The electrodes consisted of a glassy carbon working electrode, a reference electrode made of a silver wire in a 10 mм AgNO₃ solution contained by a Vycor tip and an auxiliary electrode of platinum wire. All cyclic voltammograms were referenced to the ferrocene/ ferrocenium (Fc/Fc⁺) redox couple. Spectroelectrochemistry was performed in a 40 mL DCM solution containing 0.1 M TBAH. The electrodes consisted of a Pt wire working electrode, a counterelectrode made of a platinum wire in contact with carbon felt separated from the solution by a glass frit and a silver wire as the reference electrode. UV/Vis spectra were obtained by using a StellarNet Miniature BLUE-wave UV/Vis dip probe with a tungsten/krypton light source and a 10 mm path-length tip. Elemental analysis was carried out by Midwest Microlab, LLC, Indianapolis, IN. IR spectra were recorded on a Bruker Tensor 27 FTIR spectrometer by using an attenuated total reflectance (ATR) adapter. Mass spectra were obtained at the Paul Bender Chemical Instrumentation Center of the Chemistry Department of the University of Wisconsin-Madison by using a Thermo Q Exactive™ Plus ESI-MS.

Crystallography

Crystallographic data were obtained at the Molecular Structure Laboratory of the Chemistry Department of the University of Wisconsin-Madison. Crystals were selected under oil at ambient conditions and mounted on the tip of a MiTeGen MicroMount©. Each crystal was mounted in a stream of cold nitrogen at 100(1) K and centered in the X-ray beam by using a video camera. The crystal evaluation and data collection were performed on a Bruker Quazar SMART APEX-II diffractometer with Mo_{K α} (λ = 0.71073 Å) radiation. The data were collected by using a routine to survey an entire sphere of reciprocal space and indexed by the SMART program. [21] The structures were solved by direct methods and refined by iterative cycles of least-squares refinement on F^2 followed by difference Fourier synthesis. [22] All H atoms were included in the final structure factor calculation at idealized positions and allowed to ride on the neighboring atoms with relative isotropic displacement coefficients. Single crystals of 1-5 suitable for structural determination were obtained by slow cooling a DCM/hexane mixture to -20 °C, slow diffusion of hexane into THF, and slow diffusion of hexane into Et₂O solutions, respectively. Complex 1 was treated with the





SQUEEZE function of the PLATON program to remove solvent molecules from the void space, removing 277 electrons from a void of 1168 ų, which is consistent with approximately $6.6\,\text{CH}_2\text{Cl}_2$ molecules. Complex **2** was treated with the SQUEEZE function of the PLATON program to remove solvent molecules from the void space, removing 76 electrons from a void of 263 ų, which is consistent with approximately two THF molecules.

EPR spectroscopy

EPR data were acquired with a Bruker ELEXSYS E500 EPR spectrometer with a Varian E102 microwave bridge interfaced with a Linux system. An Oxford Instruments ESR-900 continuous-flow heliumflow cryostat and an Oxford Instruments 3120 temperature controller were used to set and maintain the temperature of the sample. A Hewlett-Packard 432 A power meter was used for microwave power calibration, with measurement conditions as follows: for [1] in DCM 9.3826 GHz, 100 MHz modulation frequency, 3.000 G modulation amplitude, 3250 G center field, 3000 G sweep width, 0.5024 mW power, 70 dB gain, 20.48 ms time constant and 10 K. The simulation was performed by using EasySpin software. [24] The following parameters were used to model the data for $[1]^+$, $q_x =$ 2.105, $g_v = 2.000$, $g_z = 1.960$, $A_{xrRh} = 200$, $A_{yrRh} = 100$, $A_{zrRh} = 150$ MHz, $HStrain_x = 75$, $HStrain_y = 150$, $HStrain_z = 80$ MHz, and $S = \frac{1}{2}$ (HStrain is an anisotropic line-broadening term that accounts for unresolved hyperfine).

Computational methods

Initial coordinates of 1 and [1]⁺ were obtained from the crystallographic data for compound 1. All geometry optimizations were carried out with ORCA version 2.9.1^[25] and the BP86 exchange-correlation functional.^[26] The TZVP basis set^[27] including all electron scalar relativistic effects within the ZORA^[28] approximation were used with the TZVP/J auxiliary basis set^[29] for Rh and Bi. The SVP basis set^[27] and SVP/J auxiliary basis set^[29] were used on all remaining atoms. Solvation effects were treated with the COSMO solvation model^[30] in DCM. Tight optimization and tight self-consistent field convergence criteria were employed along with grid4 for all calculations. Frequency calculations were performed following geometry optimizations to ensure minimum energy structures. Molecular graphics were created with the UCSF Chimera package.^[31]

Synthesis and characterization

BiRh(p-OMe-form)₄ (1): Solid BiRh(TFA)₄ (52.3 mg, 0.0685 mmol) and H(p-OMe-form) (1.20 g, 4.68 mmol) were combined in a 10 mL Schlenk flask, degassed, and heated under static vacuum to 135 °C using an oil bath for 17 h, during which time the ligand became molten and the mixture turned red brown. After cooling to room temperature, the solids were purified by column chromatography on SiO_2 using hexane/EtOAc (3:2) as eluent ($R_f = 0.56$, hexane/ EtOAc 1:1). The red brown fraction was collected and dried in vacuo to give a red brown solid. Yield: 45.6 mg, 49.9 %. X-ray quality crystals of 1 were obtained overnight from a DCM/hexane solution of 1 at -20 °C. ESI-MS (positive ion, MeCN): m/z [M+H]⁺ calcd for BiRhC₆₀H₆₁N₈O₈: 1333.3471; found: 1333.3471; ¹H NMR (CDCl₃, 500 MHz): $\delta = 8.45$ (d, ${}^{3}J_{H-Rh} = 1.5$ Hz, 4H), 6.83–6.74 (m, 16H), 6.67– 6.55 (m, 16H), 3.78 (s, 12H), 3.78 ppm (s, 12H); ¹³C{¹H} NMR (CDCl₃, 125 MHz): δ = 161.7, 156.7, 155.2, 144.9, 142.1, 127.2, 121.3, 114.8, 114.2, 55.8, 55.7 ppm; IR (ATR): $\tilde{v} = 2950$ (w), 1610 (w), 1563 (w), 1533 (m), 1508 (w), 1467 (s), 1442 (w), 1332 (w), 1316 (m), 1242 (w), 1220 (s), 1218 (m), 1204 (m), 1181 (w), 1168 (w), 1104 (m), 1035 (s), 953 (w), 936 (w), 835 (s), 828 (s), 789 (w), 749 (m), 661 (w), 652 (w), 633 cm^{-1} (w); UV/Vis (DCM): λ_{max} (ϵ): 453 (8775), 544 nm (934 M $^{-1}$ cm $^{-1}$).

BiRh(p-Me-form)₄ (2): Solid BiRh(TFA)₄ (42.3 mg, 0.0553 mmol) and H(p-Me-form) (1.23 g, 5.48 mmol) were combined in a 10 mL Schlenk flask, degassed, and heated under static vacuum to 145 °C using an oil bath for 17 h, during which time the ligand became molten, and the mixture turned red brown. After cooling to room temperature, the solids were extracted with hexane/Et₂O (2:1), filtered, concentrated under reduced pressure, and purified by column chromatography on SiO₂ using hexane/Et₂O (2:1) as eluent ($R_f = 0.46$, hexane/Et₂O 1:1). The red orange fraction was collected and dried in vacuo to give a red orange solid. Yield: 26.0 mg, 38.9%. X-ray quality crystals of 2 were obtained by layering a concentrated THF solution of 2 with hexane. ESI-MS (positive ion, MeCN): m/z [M+H]⁺ calcd for BiRhC₆₀H₆₁N₈: 1205.3873; found: 1205.3875; ¹H NMR (CDCl₃, 500 MHz): $\delta = 8.44$ (d, ${}^{3}J_{H-Rh} = 1.6$ Hz, 4H), 6.97 (d, J=8.0 Hz, 8H), 6.87 (d, J=8.0 Hz, 8H), 6.76 (d, J=8.0 Hz, 8 H), 6.55 (d, J = 8.0 Hz, 8 H), 2.25 ppm (s, 24 H); $^{13}C(^{1}H)$ NMR $(CDCl_3, 125 \text{ MHz}): \delta = 161.7, 149.1, 146.0, 133.6, 131.3, 129.9, 129.4,$ 126.3, 120.1, 21.0, 20.9 ppm; UV-Vis (DCM) λ_{max} (ϵ): 464 (4047), 558 nm (373 M⁻¹ cm⁻¹).

BiRh(form)₄ (3): Solid BiRh(TFA)₄ (50.6 mg, 0.0663 mmol) and H(form) (1.07 g, 5.45 mmol) were combined in a 10 mL Schlenk flask, degassed, and heated under static vacuum to 130°C using an oil bath for 17 h, during which time the ligand became molten, and the mixture turned red brown. After cooling to room temperature, excess ligand was removed by sublimation at 120°C under reduced pressure. The remaining brown solids were recrystallized from Et₂O/hexane, filtered, washed with small amounts of cold hexane, and dried in vacuo to give a red brown solid. Yield: 43.6 mg, 60.2%. X-ray quality crystals of 3 were obtained by layering a concentrated THF solution of 3 with hexane. ESI-MS (positive ion, MeCN): m/z [M+H]⁺ calcd for BiRhC₅₂H₄₅N₈: 1093.2621; found: 1093.2629; ¹H NMR (CDCl₃, 500 MHz): $\delta = 8.57$ (d, ${}^{3}J_{H-Rh} = 1.8$ Hz, 4H), 7.18 (dd, J=7.8, 7.4 Hz, 8H), 7.10–7.05 (m, 12H), 6.96 (t, J=7.5 Hz, 4H), 6.88 (d, J=8.5 Hz, 8H), 6.67 ppm (dd, J=7.8, 2.0 Hz, 8 H); $^{13}\text{C}\{^1\text{H}\}$ NMR (CDCl3, 125 MHz): $\delta\!=\!161.9$, 151.2, 148.1, 129.4, 128.8, 126.3, 124.2, 122.2, 120.2 ppm; IR (ATR): $\tilde{\nu} = 1555$ (s), 1527 (s), 1484 (s), 1449 (w), 1334 (s), 1262 (w), 1216 (s), 1178 (w), 1079 (m), 1028 (m), 962 (s), 933 (s), 815 (m), 767 (s), 751 (s), 700 (s), 689 656 cm⁻¹ (w); UV/Vis (DCM): λ_{max} (ϵ): 460 (4736), 551 nm(402 M⁻¹ cm⁻¹).

BiRh(p-Cl-form)₄ (4): Solid BiRh(TFA)₄ (38.3 mg, 0.0501 mmol) and H(p-Cl-form) (1.21 g, 4.56 mmol) were combined in a 10 mL Schlenk flask, degassed, and heated under static vacuum to 180 °C using an oil bath for 17 h, during which time the ligand became molten, and the mixture turned red brown. After cooling to room temperature, the solids were extracted with hexane/Et₂O (2:1), filtered, concentrated under reduced pressure, and purified by column chromatography on SiO₂ using hexane/Et₂O (2:1) as eluent $(R_f = 0.42, \text{ hexane/Et}_2\text{O } 1:1)$. The red orange fraction was collected and dried in vacuo to give a red orange solid. Yield: 35.2 mg, 51.4%. X-ray quality crystals of 4 were obtained by layering a concentrated Et₂O solution of 4 with hexane. ESI-MS (positive ion, MeCN): $m/z [M+H]^+$ calcd for BiRhC₅₂H₃₇N₈Cl₈: 1364.9503; found: 1364.9506; ¹H NMR (CDCl₃, 500 MHz): $\delta = 8.51$ (d, ${}^{3}J_{H-Rh} = 1.6$ Hz, 4H), 7.16 (d, J=8.4 Hz, 8H), 7.09 (d, J=8.4 Hz, 8H), 6.72 (d, J=8.4 Hz, 8 H), 6.56 ppm (d, J=8.4 Hz, 8 H); ${}^{13}C\{{}^{1}H\}$ NMR (CDCl₃, 125 MHz): δ = 161.9, 149.1, 146.0, 130.7, 129.8, 129.4, 128.4, 127.0, 121.3 ppm; UV/Vis (DCM): λ_{max} (ϵ): 462 (11795), 557 nm $(1429 \text{ M}^{-1} \text{ cm}^{-1}).$

 $BiRh(p-CF_3-form)_4$ (5): Solid $BiRh(TFA)_4$ (51.9 mg, 0.0680 mmol) and $H(p-CF_3-form)$ (1.50 g, 4.51 mmol) were combined in a 10 mL





Schlenk flask, degassed, and heated under static vacuum to 165 °C using an oil bath for 17 h, during which time the ligand became molten, and the mixture turned red brown. After cooling to room temperature, the solids were extracted with hexane/DCM (2:1), filtered, concentrated under reduced pressure, and purified by column chromatography on SiO₂ by using hexane/DCM (2:1) as eluent (R_f =0.42, hexane/DCM 2:1). The red orange fraction was collected and dried in vacuo to give a red orange solid. Yield: 45.0 mg, 40.4%. X-ray quality crystals of 5 were obtained by layering a concentrated Et₂O solution of 5 with hexane; elemental analysis calcd for BiRhC₆₀H₃₆N₈F₂₄: (1636.8): C 44.0, H 2.2, N 6.9; found: C 43.8, H 2.2, N 6.7; ESI-MS (positive ion, MeCN): m/z [M+H]⁺ calcd for $BiRhC_{60}H_{36}N_8F_{24}$: 1637.1612; found: 1637.1631; 1H NMR (CDCl₃, 500 MHz): $\delta = 8.74$ (d, ${}^{3}J_{H-Rh} = 1.6$ Hz, 4H), 7.47 (d, J = 8.3 Hz, 8H), 7.38 (d, J = 8.3 Hz, 8H), 6.86 (d, J = 8.3 Hz, 8H), 6.79 ppm (d, J =8.3 Hz, 8 H); 13 C{ 1 H} NMR (CDCl $_{3}$, 125 MHz, ppm): δ = 162.4 (s), 153.1 (s), 149.7 (s), 127.7 (q, ${}^{2}J_{C-F} = 33$ Hz), 127.3 (q, ${}^{3}J_{C-F} = 4$ Hz), 126.8 (q, $^{3}J_{C-F} = 4$ Hz), 125.9 (q, $^{2}J_{C-F} = 33$ Hz), 125.5 (s), 124.3 (q, $^{1}J_{C-F} =$ 272 Hz), 124.1 (q, ${}^{1}J_{C-F}$ = 272 Hz), 120.0 ppm (s); ${}^{19}F\{{}^{1}H\}$ NMR (CDCl₃, 376 MHz): $\delta = -62.0$, -62.3 ppm; IR (ATR): 1610 (w), 1563 (s), 1538 (m), 1508 (m), 1316 (s), 1218 (m), 1181 (m), 1160 (m), 1105 (s), 1065 (s), 1010 (w), 979 (w), 936 (w), 835 (m), 661 (w), 633 cm⁻¹ (w); UV/ Vis (DCM): λ_{max} (ε): 457 (5965), 553 nm (812 M⁻¹ cm⁻¹).

Acknowledgements

We thank Dr. Amanda Corcos for obtaining EPR data, Dr. Charles Fry, Prof. Hans Reich, and Prof. Thomas Brunold for helpful discussions. We thank the NSF for financial support of this research through CHE-1300464. The purchase of the Thermo-Q Exactive[™] Plus in 2015 was partially funded by NIH 1S100D020022−1 to the Department of Chemistry.

Keywords: bismuth \cdot heterobimetallic complexes \cdot magnetic anisotropy \cdot metal-metal bonds \cdot rhodium

- [1] a) V. A. Kulbachinskii, A. Y. Kaminskii, K. Kindo, Y. Narumi, K. Suga, P. Lostak, P. Svanda, *Phys. B* 2002, *311*, 292–297; b) Y. L. Chen, J. H. Chu, J. G. Analytis, Z. K. Liu, K. Igarashi, H. H. Kuo, X. L. Qi, S. K. Mo, R. G. Moore, D. H. Lu, M. Hashimoto, T. Sasagawa, S. C. Zhang, I. R. Fisher, Z. Hussain, Z. X. Shen, *Science* 2010, *329*, 659–662; c) Y. S. Hor, P. Roushan, H. Beidenkopf, J. Seo, D. Qu, J. G. Checkelsky, L. A. Wray, D. Hsieh, Y. Xia, S. Y. Xu, D. Qian, M. Z. Hasan, N. P. Ong, A. Yazdani, R. J. Cava, *Phys. Rev. B* 2010, *81*, 195203; d) W. Liu, D. West, L. He, Y. Xu, J. Liu, K. Wang, Y. Wang, G. Laan, R. Zhang, S. Zhang, K. L. Wang, *ACS Nano* 2015, *9*, 10237–10243; e) S. M. Clarke, D. E. Freedman, *Inorg. Chem.* 2015, *54*, 2765–2771.
- [2] a) J. H. Thurston, K. H. Whitmire, *Inorg. Chem.* 2003, 42, 2014–2023;
 b) J. H. Thurston, A. Kumar, C. Hofmann, K. H. Whitmire, *Inorg. Chem.* 2004, 43, 8427–8436;
 c) J. H. Thurston, D. Trahan, T. Ould-Ely, K. H. Whitmire, *Inorg. Chem.* 2004, 43, 3299–3305;
 d) E. V. Dikarev, H. Zhang, B. Li, *J. Am. Chem.* 2005, 277, 6156–6157;
 e) V. Stavila, J. H. Thurston, K. H. Whitmire, *Inorg. Chem.* 2009, 48, 6945–6951;
 f) T. C. Stamatatos, K. Oliver, K. A. Abboud, G. Christou, *Inorg. Chem.* 2011, 50, 5272–5282;
 g) M. Hołyńska, *Inorg. Chem. Commun.* 2012, 20, 322–325;
 h) I. Bulimestru, S. Shova, N. Popa, P. Roussel, F. Capet, R. Vannier, N. Djelal, L. Burylo, J. Wignacourt, A. Gulea, K. H. Whitmire, *Chem. Mater.* 2014, 26, 6092–6103.
- [3] E. V. Dikarev, T. G. Gray, B. Li, Angew. Chem. Int. Ed. 2005, 44, 1721 1724; Angew. Chem. 2005, 117, 1749 1752.
- [4] a) A. S. Filatov, M. Napier, V. D. Vreshch, N. J. Sumner, E. V. Dikarev, M. A. Petrukhina, *Inorg. Chem.* 2012, *51*, 566–571; b) T. L. Sunderland, J. F.

www.chemeurj.org

- Berry, *Dalton Trans.* **2016**, *45*, 50–55; c) T. L. Sunderland, J. F. Berry, *J. Coord. Chem.* **2016**, 1–14.
- [5] a) L. J. Clouston, V. Bernales, R. C. Cammarota, R. K. Carlson, E. Bill, L. Gagliardi, C. C. Lu, *Inorg. Chem.* 2015, *54*, 11669 11679; b) R. J. Eisenhart, P. A. Rudd, N. Planas, D. W. Boyce, R. K. Carlson, W. B. Tolman, E. Bill, L. Gagliardi, C. C. Lu, *Inorg. Chem.* 2015, *54*, 7579 7592.
- [6] J. F. Berry, E. Bill, E. Bothe, F. A. Cotton, N. S. Dalal, S. A. Ibragimov, N. Kaur, C. Y. Liu, C. A. Murillo, S. Nellutla, J. M. North, D. Villagrán, J. Am. Chem. Soc. 2007, 129, 1393–1401.
- [7] F. A. Cotton, C. A. Murillo, R. A. Walton in Multiple Bonds Between Metal Atoms, 3rd ed., Springer Science and Business Media, New York, 2005.
- [8] a) C. Lin, J. D. Protasiewicz, T. Ren, Inorg. Chem. 1996, 35, 7455-7458;
 b) T. Ren, C. Lin, E. J. Valente, J. D. Zubkowski, Inorg. Chim. Acta 2000, 297, 283-290;
 c) C. Lin, J. D. Protasiewicz, E. T. Smith, T. Ren, J. Chem. Soc. Chem. Commun. 1995, 2257-2258;
 d) C. Lin, J. D. Protasiewicz, E. T. Smith, T. Ren, Inorg. Chem. 1996, 35, 6422-6428;
 e) C. Lin, T. Ren, E. J. Valente, J. D. Zubkowski, E. T. Smith, Chem. Lett. 1997, 753-754;
 f) T. Ren, Coord. Chem. Rev. 1998, 175, 43-58;
 g) C. Lin, T. Ren, E. J. Valente, J. D. Zubkowski, J. Organomet. Chem. 1999, 579, 114-121.
- [9] R. G. Pearson, J. Am. Chem. Soc. 1988, 110, 2092 2097.
- [10] J. L. Bear, C. L. Yao, R. S. Lifsey, J. D. Korp, K. M. Kadish, *Inorg. Chem.* 1991, 30, 336–340.
- [11] M. J. McGlinchey, Inorg. Chem. 1980, 19, 1392-1394.
- [12] J. San Filippo, Inorg. Chem. 1972, 11, 3140-3143.
- [13] a) F. A. Cotton, Z. Li, C. A. Murillo, P. V. Poplaukhin, J. H. Reibenspies, J. Cluster Sci. 2008, 19, 89-97; b) F. A. Cotton, J. H. Matonic, C. A. Murillo, Inorg. Chim. Acta 1997, 264, 61-65; c) F. A. Cotton, T. Ren, J. Am. Chem. Soc. 1992, 114, 2237-2242; d) F. A. Cotton, T. Ren, J. Am. Chem. Soc. 1992, 114, 2495-2502; e) P. Piraino, G. Bruno, S. L. Schiavo, F. Laschi, P. Zanello, Inorg. Chem. 1987, 26, 2205-2211; f) F. A. Cotton, L. M. Daniels, C. A. Murillo, Angew. Chem. Int. Ed. Engl. 1992, 31, 737-738; Angew. Chem. 1992, 104, 795-796.
- [14] H. M. McConnell, J. Chem. Phys. 1957, 27, 226-229.
- [15] R. K. Harris in Nuclear Magnetic Resonance Spectroscopy: A Physiocochemical View, Longman, London, 1986.
- [16] G. A. Bain, J. F. Berry, J. Chem. Educ. 2008, 85, 532.
- [17] O. Kahn in Molecular Magnetism, Wiley, New York, 1993.
- [18] G. L. Manni, A. L. Dzubak, A. Mulla, D. W. Brogden, J. F. Berry, L. Gagliardi, Chem. Eur. J. 2012, 18, 1737 – 1749.
- [19] Small similar effects do exist in organic compounds. For example, the relatively low-energy $n \rightarrow \pi^*$ excitations in pyridine contributes to the o-H atoms appearing approximately 1 ppm downfield of the m- and p-H atoms. Protonation of pyridine (i.e., elimination of the $n \rightarrow \pi^*$ excitation) raises the chemical shifts of the m- and p-H atoms uniformly by 0.6 0.7 ppm, but only raises the o-H atom chemical shifts by 0.3 ppm. See: J. A. Gowland, R. A. McClelland, Can. J. Chem. 1979, 57, 2140.
- [20] W. Bradley, I. Wright, J. Chem. Soc. 1956, 640-648.
- [21] Bruker-AXS, SMART Program, Madison, Wisconsin, USA, 2009.
- [22] a) G. Sheldrick, Acta Crystallogr. Sect. A 2008, 64, 112–122; b) O. V. Dolomanov, L. J. Bourhis, R. J. Gildea, J. A. K. Howard, H. Puschmann, J. Appl. Crystallogr. 2009, 42, 339–341.
- [23] A. Spek, *Acta Crystallogr. Sect. D* **2009**, *65*, 148–155.
- [24] S. Stoll, A. Schweiger, J. Magn. Reson. 2006, 178, 42-55.
- [25] F. Neese, ORCA: an ab initio, Density Functional and Semiempirical program package, University of Bonn, Bonn, 2006.
- [26] A. D. Becke, J. Chem. Phys. 1993, 98, 5648.
- [27] D. A. Pantazis, X. Chen, C. R. Landis, F. Neese, J. Chem. Theory Comput. 2008, 4, 908 – 919.
- [28] C. V. Wüllen, J. Chem. Phys. 1998, 109, 392-399.
- [29] K. Eichkorn, O. Treutler, H. Öhm, M. Häser, R. Ahlrichs, Chem. Phys. Lett. 1995, 240, 283 – 290
- [30] a) S. Sinnecker, A. Rajendran, A. Klamt, M. Diedenhofen, F. Neese, J. Phys. Chem. A 2006, 110, 2235–2245; b) A. Klamt, G. Schuurmann, J. Chem. Soc. Perkin Trans. 2 1993, 799–805.
- [31] E. F. Pettersen, T. D. Goddard, C. C. Huang, G. S. Couch, D. M. Greenblatt, E. C. Meng, T. E. Ferrin, J. Comput. Chem. 2004, 25, 1605 – 1612.

Received: August 23, 2016 Published online on November 3, 2016